Catalysis Today 157 (2010) 55–60

Contents lists available at ScienceDirect

Catalysis Today

journal homepage: www.elsevier.com/locate/cattod

Oxygen mobility of Pt-promoted doped CeO_2–ZrO_2 solid solutions: Characterization and effect on catalytic performance in syngas generation by fuels oxidation/reforming

V. Sadykov[a,b,*], V. Muzykantov[a], A. Bobin[a,c], N. Mezentseva[a], G. Alikina[a], N. Sazonova[a], E. Sadovskaya[a], L. Gubanova[a], A. Lukashevich[a], C. Mirodatos[c]

[a] Boreskov Institute of Catalysis, Novosibirsk, Russia
[b] Novosibirsk State University, Novosibirsk, Russia
[c] Institut de Recherches sur la catalyse et l'environnement de Lyon, France

ARTICLE INFO

Keywords:
Doped ceria–zirconia
Supported Pt
Oxygen isotope exchange
CH_4
Acetone
Partial oxidation
Dry and autothermal reforming
Syngas

ABSTRACT

For nanocrystalline ceria–zirconia samples doped with rare-earth (Gd, Pr, La) cations prepared via modified Pechini route and promoted by Pt supported by wet impregnation, parameters characterizing their oxygen mobility and reactivity were estimated from results of oxygen isotope exchange experiments in both isothermal and temperature-programmed modes using different procedures. Observed trends in variation of oxygen exchange parameters with the type and content of a dopant were explained with a due regard for the real structure and surface properties of samples earlier characterized in detail. For the reaction of partial oxidation and dry reforming of methane in diluted feeds, catalytic activity correlates both with Pt dispersion and oxygen mobility. For the reactions of acetone autothermal reforming and CH_4 dry reforming in realistic feeds, catalytic activity is mainly determined by the surface/bulk oxygen mobility responsible for coking suppression.

1. Introduction

Ceria–zirconia oxide solid solutions with supported precious metals are promising as catalysts for automotive control, transformation of hydrocarbons or oxygenates into syngas, solid oxide fuel cell anodes etc. [1–4]. The lattice oxygen mobility is an important factor ensuring a high efficiency and stable performance of these systems. The incorporation of rare-earth cations into Ce–Zr–O oxides stabilizes their structure and tunes the oxygen mobility [1,5–7]. Isotope oxygen heteroexchange is one of the most straightforward methods to characterize the oxygen mobility and reactivity [8–18]. However, papers devoted to systematic estimation and analysis of the oxygen exchange parameters for series of Pt-supported doped ceria–zirconia samples are still rare [5,7]. Studies of the real structure and surface properties of ceria–zirconia solid solutions doped by La, Gd or Pr cations carried out last years by authors [7,19–23] provide required basis for such an analysis. This paper is devoted to estimation of parameters characterizing the oxygen mobility in Pt-promoted nanocrystalline ceria–zirconia solid solutions doped by La, Gd, or Pr by using results of isotope exchange experiments in both isothermal and temperature-programmed modes. Factors controlling mobility and reactivity of oxygen were analyzed with a due regard for these samples structure and surface properties. The impact of oxygen mobility on these catalysts performance in partial oxidation of methane (POM), its dry reforming (DR) and autothermal reforming (ATR) of acetone into syngas at short contact times was considered. These three reactions were selected here for comparison because they are known to differ substantially by the coking ability (ATR > DR > POM) [24–27], thus presenting a good possibility for elucidating the relevance of the oxygen mobility for the same series of samples with a due regard for the reaction specificity.

2. Experimental

Dispersed samples of ceria–zirconia based solid solutions $(Ce_{0.5}Zr_{0.5})_{1-x}Ln_xO_{3-\delta}$ (Ln = Pr, La or Gd, $x = 0.05$–0.3) were prepared by polymerized complex precursor route and calcined at 700 °C [2,5]. Pt (1.4 wt.%) was supported from H_2PtCl_6 solution by incipient wetness impregnation followed by drying and calcination at 500 °C for 2 h. Results of detailed characterization of the real structure and surface properties of samples by using combination

* Corresponding author at: Boreskov Institute of Catalysis SB RAS, Prosp. Acad. Lavrentieva, 5, 630090 Novosibirsk, Russia. Tel.: +7 383 3308763; fax: +7 383 3308056.
E-mail addresses: sadykov@catalysis.ru, vasadykov@mail.ru (V. Sadykov).

0920-5861/$ – see front matter © 2010 Elsevier B.V. All rights reserved.
doi:10.1016/j.cattod.2010.03.064

of diffraction (TEM, XRD, neutronography), spectroscopic (EXAFS, SIMS, XPS, FTIRS of adsorbed CO molecules) and magnetic methods are given elsewhere [5,7,19–23]. Specific surface area of samples varies in the range of 50–150 m^2/g increasing with the dopant content and decreasing after Pt supporting [4–7]. All kinetic parameters reported in the paper if required were related per the surface unit of samples.

Oxygen isotope exchange experiments with powdered samples were carried out in a static installation ($V = 680\,cm^3$) with on-line control of the gas phase isotope composition by QMS-200 (Stanford Research Systems, USA) mass-spectrometer in two modes:

1. Isothermal isotope exchange (IIE) at pO_2 1.5–4.5 Torr at 360–650 °C.
2. Temperature-programmed isotope exchange (TPIE) with the temperature ramp 5 K/min from 100 to 750 °C.

The initial ^{18}O content in the gas phase was equal to 96%. Before experiments, samples were pretreated for 2 h under air at 650 °C.

Activation energy of exchange was estimated using IIE data as well as data of TPIE following approach suggested by Cheselske et al. [28].

Catalytic activity of powdered samples (fractions 0.25–0.5 mm) in the reactions of autothermal reforming of acetone (ATR, feed 0.7% C_3H_6O + 0.5% H_2O + 0.5% O_2 in He), partial oxidation (POM, 1% CH_4 + 0.5% O_2 in He) of CH_4 and its dry reforming (DR, 1% CH_4 + 1% CO_2 in He) at short contact times (0.5–25 ms) was studied at temperatures up to 900 °C in a flow installation following earlier described procedures [5–7]. For POM, efficient first-order reaction rate constants were calculated using the integral equation for the plug-flow reactor which was shown to satisfactory describe the experimental data [5] in agreement with results of Wei and Iglesia [29]. Thus, specific rates of methane transformation, related to its inlet content in the feed, were obtained, and their multiplying by the hydrogen selectivity yields the rates of hydrogen generation used for comparison of the samples activity [5]. For the ATR of acetone, due to difficulties in closing the carbon balance, only integral rates of hydrogen generation at 880 °C related to the specific surface area of catalysts were estimated using the steady-state hydrogen concentration in the products and feed rate [20].

To estimate performance in DR in realistic feeds (CH_4 content 7–20%) without impact of heat and mass transfer effects, catalytic activity was tested using thin (~10 μm) catalytic layers supported on the walls of single-channel triangular corundum substrate as described earlier [30,31].

3. Theory

The redistribution of the isotope molecules during heteroexchange $^{18}O_i{}^{16}O_{2-i}$ ($i = 0, 1, 2$) characterized by their molar fractions x_i ($x_0 + x_1 + x_2 = 1$) is described by isotope-kinetic equations [11–14]:

$$\frac{N}{S}\frac{d\alpha}{dt} = -R(\alpha - \alpha_s) \tag{1}$$

$$\frac{N}{S}\frac{dx_1}{dt} = K_1[2\alpha(1-\alpha) - x_1] + K_2[\alpha(1-\alpha_s) + \alpha_s(1-\alpha) - x_1] + K_3[2\alpha_s(1-\alpha_s) - x_1] \tag{2}$$

Here N is the number of O_2 molecules, S is the surface area of oxide, t is the time, $\alpha = 0.5x_1 + x_2$-isotope fraction, $R = 0.5K_2 + K_3$ is the rate of heteroexchange, k_1, k_2 and k_3 are the rates of exchange of the 1st, 2nd and 3rd type (with participation of 0, 1 and 2 surface oxygen atoms, respectively [11–14]), their sum giving the total rate of exchange R.

For a complete description of the isotope redistribution, differential equations reflecting the isotope transfer in the solid phase should be added to this system:

$$\frac{N_s}{S}\frac{\partial\alpha_s}{\partial t} = R(\alpha - \alpha_s) - r_D\frac{N_e}{S}\left.\frac{\partial\alpha_v}{\partial\eta}\right|_{\eta=0} \tag{3}$$

$$\frac{\partial\alpha_v}{\partial t} = r_D\frac{\partial^2\alpha_v}{\partial\eta^2} \tag{4}$$

With the initial and boundary conditions:

$$t = 0: \quad \alpha = \alpha^0, \quad \alpha_s = \alpha_v = \alpha_s{}^0; \quad \eta = 0: \quad \alpha_v = \alpha_s$$

where α_v is the fraction of ^{18}O in the oxide bulk, N_s and N_e are the number of oxygen atoms in the surface layer of oxide and the number of exchangeable atoms in the bulk of the oxide, respectively; η is the reduced depth (z) of the oxide layer $\eta = z/h$, where h is the characteristic size of oxide particles; $r_D = D/h^2$ is the effective diffusion coefficient (diffusion relaxation constant), D is the oxygen self-diffusion coefficient.

By transformation of isotope Eqs. (1) and (2), so called isotope-mechanistic equation (5) without time was derived:

$$\ln\left[\frac{v+b}{v^0+b}\right] = -a\ln\left(\frac{s}{s^0}\right), \tag{5}$$

Here $v = z/s^2$, $s = \alpha - \alpha_s$, $z = x_2 - \alpha^2 x_2$, x_2 is the fraction of $^{18}O_2$ molecules, and parameters a and b are determined by the type of mechanism [11]:

$$a = 2\frac{k}{r} = \frac{\kappa_2 + 2\kappa_3 - 1}{0.5\kappa_2 + \kappa_3}$$

$$b = \frac{k_3}{2r - k} = \frac{\kappa_3}{\kappa_2 + 2\kappa_3 - 1}$$

The depth of isotope penetration from the gas phase into the oxide in the course of TPIE can be characterized by the value N_X determined from the relation:

$$2N\alpha^0 + N_X\alpha_S^0 = \alpha(2N + N_X) \tag{6}$$

The value N_X is related to the average depth of isotope incorporation into the solid phase (l_α) by relation $N_X = n_O{}^* S^* l_\alpha$ (here n_O is the number of oxygen atoms in the unit volume of oxide). This quantity termed as "dynamic degree of isotope exchange" [4,5] is expressed in relative units $X_S = N_X/N_S$ and $X_V = N_X/N_V$, corresponding, respectively, to the number of exchanged oxygen monolayers X_s (1 monolayer = 1.4×10^{19} atoms/m^2) and the exchanged fraction of the bulk oxygen, X_v.

Cheselske et al. [28,32] derived equation to estimate apparent activation energy of heteroexchange in experiments with a linear temperature ramp and uniform by reactivity species:

$$E = -\left[RT^2\frac{d\alpha/dT}{\alpha - \gamma}\right]_I \tag{7}$$

Here, $-d\alpha/dT$ is taken at the inflection point where it achieves a maximum value, α is the respective isotope fraction at this point, γ is the equilibrium isotope fraction.

4. Results and discussion

4.1. Oxygen isotope exchange

Temperature-programmed isotope exchange (*TPIE*): For all samples of fluorite-like oxides including those promoted by Pt, linearization of results in coordinates of isotope-mechanistic Eq. (5) revealed domination of the 3rd type of mechanism (a share in the range of 0.7–0.9), without any impact of the 1st type of exchange.

Estimation of the dynamic degree of exchange [5–7] revealed that at temperatures below 600 °C, the oxygen exchange is limited

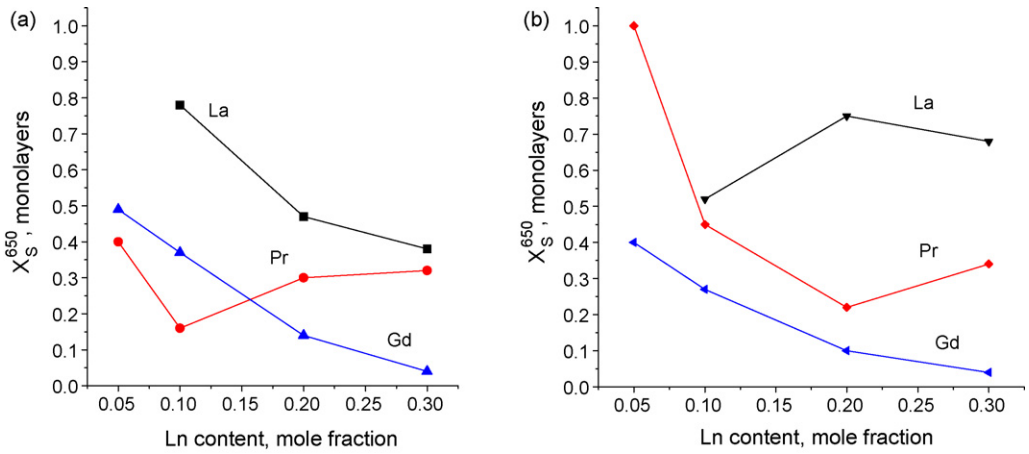

Fig. 1. Dependence of dynamic degree of exchange X_S on the dopant content for samples of $Ln_x(Ce_{0.5}Zr_{0.5})_{1-x}O_{2-y}$ (a) and $Pt/Ln_x(Ce_{0.5}Zr_{0.5})_{1-x}O_{2-y}$ (b). PO_2 2.5 Torr.

to the surface layers (X_S below 1 monolayer) due to much faster surface reaction and diffusion as compared to the bulk diffusion [16–18,33]. At higher temperatures incorporation of isotope into the bulk of oxide particles occurs rather fast, so, for some samples, i.e. for $Pt/Ce_{0.5}Zr_{0.5}O_{2-x}$ sample, X_S achieves 4–5 monolayers at 700–750 °C [5,7]. To characterize mainly the surface/near surface oxygen mobility, 650 °C was selected as the temperature of comparison [4–7]. Indeed, at this temperature for majority of samples considered here X_S is below a monolayer (Fig. 1), thus mainly reflecting the oxygen migration within the surface/near-surface layers. As integral parameter, X_s depends upon all factors controlling dynamics of the surface reaction and diffusion in solid, namely, the sample pretreatment, gas phase oxygen concentration, temperature ramp, etc. For the same sample in strictly fixed experimental conditions, reproducibility of X_s values is ca. 10 rel.%. Comparison of X_S for different samples is the most informative when their specific surface area (particle sizes) and composition do not differ substantially [4–7], as is the case of the present studies.

For the undoped (parent) samples $Ce_{0.5}Zr_{0.5}O_{2-x}$ and $Pt/Ce_{0.5}Zr_{0.5}O_{2-x}$, X_S values at 650 °C and 2.5 Torr O_2 are equal to 0.5 and 1.7, respectively, i.e. being in general higher than for doped samples. This feature was explained by well-known microheterogeneity of the structure of nanocrystalline ceria–zirconia solid solutions consisting of domain enriched by Zr and Ce cations, respectively [34]. This microheterogeneity generates Frenkel-type defects (pairs anion vacancy-oxygen interstitial) revealed in these oxides by detailed neutronographic studies of Mamontov et al. [34]. Such defects decrease the activation barriers for the oxygen diffusion and provide surface sites with a low oxygen bonding strength more active in the oxygen exchange [5,35]. Extended defects present at domain boundaries in $Ce_{0.5}Zr_{0.5}O_{2-x}$ sample and detected also as microstrains by neutron diffraction data analysis [21,23] can also provide paths for facile oxygen migration due to strongly distorted coordination polyhedra in their vicinity. Doping by smaller Pr and Gd cations provides more uniform distribution of Ce and Zr cations [4,6], thus decreasing density of Frenkel-type defects and microstrains and, as the result, decreasing oxygen mobility [5,21]. On the other hand, for largest La cations, X_S increases from 0.5 for undoped sample to 0.8 for moderate (xLa = 0.1) doping level (Fig. 1). In this case, the increase of the lattice parameter accompanied by the decrease of the surface Ce–O bond strength as revealed by SIMS [7,20] appears to be responsible for the increase of X_S for this moderately doped sample.

According to EXAFS data [19–21,23], for samples doped by Gd or La, symmetry and average coordination numbers (CN) for Zr–O and Ce–O spheres increase with the dopant content, while Ce–O sphere contracts, which suggests strengthening of Ce–O bond and disappearance of "free" anion vacancies near Ce cations caused by a complex rearrangement of coordination polyhedra. Usually, for ceria–zirconia solid solutions distortion of Zr–O and Ce–O spheres and lattice expansion leading to appearance of longer (and, hence, weaker) metal–oxygen bonds are considered as the most important factors controlling oxygen mobility [1,6,7,19–21,23]. Hence, clear expressed trend in declining of X_S with the doping level for Gd- or La-containing samples can be explained by such complex rearrangement of coordination spheres and disappearance of "free" oxygen vacancies.

For Pr-doped samples some increase of X_S at a high Pr content can be explained by increasing the Pr^{4+} share which favors mixed ionic-electronic conductivity via chains of Pr^{3+}–Pr^{4+} cations, and, hence, enhanced oxygen mobility, perhaps, along domain boundaries enriched by Pr cations [19–22].

Effect of Pt supporting on X_S (Fig. 1b) depends upon the type and content of doping cation. This suggests specific interaction of Pt with the surface sites/dopants, including, perhaps, even rearrangement of the surface layer caused by leaching of basic-type Ln^{3+} cations during incipient wetness impregnation by acid H_2PtCl_6 solutions and incorporation of Pt^{n+} cations into the surface vacant sites. For undoped sample, high values of X_S (~1.7 at 650 °C [5]) was explained by a high density of microstrains and Frenkel-type defects taking parts in stabilization of ionic Pt forms [5,7,20]. For doped samples, a minor (if any) effect of Pt supporting for Gd-doped samples appears to correlate with mainly subsurface location of small Gd cations, while the strongest effect is observed for samples doped with the biggest La cations segregated in the surface layer [20]. The most positive effect of Pt supporting on X_S, especially at a low dopant content, is observed for Pr-doped samples. This seems to correlate with the highest ability of $Pr^{3+/4+}$ cations to stabilize Pt as 2+/4+ cations [20]. Incorporation of these Pt cations into the subsurface/near surface positions as well as into domain boundaries is expected to generate oxygen vacancies as well as to enhance mixed ionic-electronic conductivity along Pr^{3+}/Pr^{4+} chains thus facilitating oxygen diffusion [20].

Estimation of E_a of heteroexchange by Eq. (7) (vide supra) helps to elucidate the effect of doping cations on the reactivity of surface sites. In typical experiments inflection point is situated at temperatures ~600–700 °C, thus being close to the temperature range of X_S estimation. Hence, estimated in such a way activation energy can be mainly considered as characteristic of the surface reaction steps. For samples without Pt, E_a of isotope exchange is higher for doped samples reflecting variation of the real structure (disappearance of extended defects at domain boundaries, more symmetric

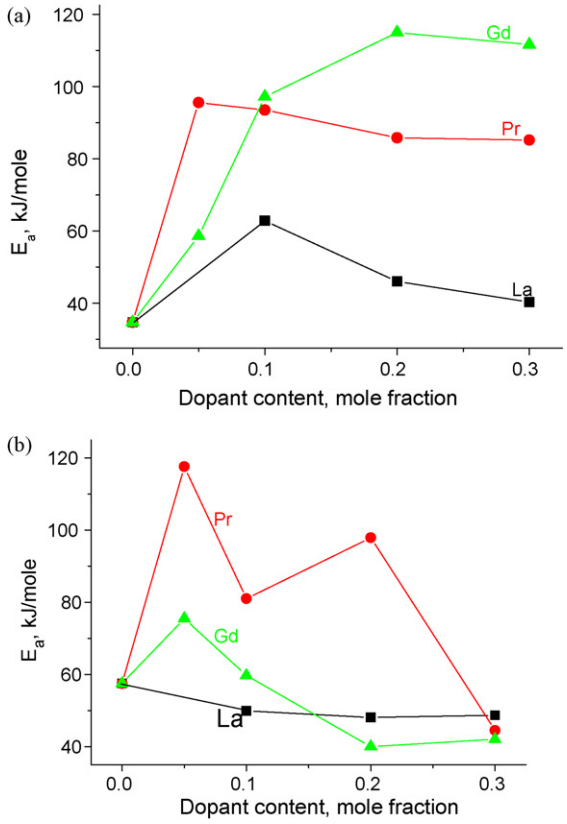

Fig. 2. Effect of dopant content in $Ln_x(Ce_{0.5}Zr_{0.5})_{1-x}O_{2-y}$ (a) and $Pt/Ln_x(Ce_{0.5}Zr_{0.5})_{1-x}O_{2-y}$ (b) samples on E_a estimated by approach of Hall et al.

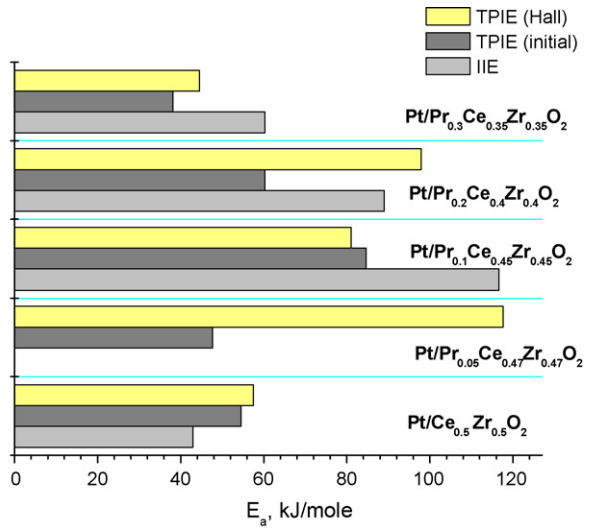

Fig. 3. Comparison of E_a estimated by different procedures for Pt/Pr–Ce–Zr–O samples.

and dense coordination sphere of Ce cations in the surface layer) increasing the Ce–O bond strength and decreasing the density of oxygen vacancies in the surface layer. Decrease of E_a with increasing the size of doping cation Gd < Pr < La (and, hence, increasing the lattice parameter [4,6,7,21]) agrees with this suggestion, since a longer (and, hence, weaker) Ce–O bond strength suggests a lower activation barrier for its rupture as well as a higher density of anion vacancies at chemical equilibrium with the gas phase oxygen.

Pt supporting effect on E_a clearly depends upon the type and content of doping cation (Fig. 2b). Pt supporting on undoped Ce–Zr–O sample increases apparent activation energy (Fig. 2b). Since Pt sites are known to be much more active in oxygen isotope exchange than ceria–zirconia surface centers [16–18,33], this suggests that thus estimated E_a is mainly determined by such steps as oxygen spillover from the Pt to support and/or surface/near surface diffusion. Estimation by fitting SSITKA data for Pt/La–Ce–Zr–O sample revealed that at 650 °C specific rates of exchange on Pt and Pt-support spillover are 1–2 order of magnitude higher than the rates of surface diffusion and exchange on support, the latter being comparable [33]. Hence, the temperature dependence of the exchange rate on Pt-supported samples should be determined mainly by the isotope surface diffusion from the Pt clusters to surrounding oxide regions.

For the largest (and, hence, the most basic) La cation, E_a only decreases with the doping level (Fig. 2b). Since fraction of oxidic Pt forms (oxidic clusters, isolated Pt^{2+} species, including those incorporated into the surface/subsurface layers and domain boundaries) increases with La content [6,7,20], this implies that barriers for the O_2 dissociation and surface/near-surface diffusion are decreased due to such action of Pt oxidic forms. This can be explained by generation of oxygen vacancies due to Pt^{2+} incorporation into the surface layer [6,7,19,21,33,36].

For Gd-doped samples Pt supporting decreases E_a for all doping levels (Fig. 2b). This can be also explained by the same mechanism of oxygen vacancies generation due to Pt^{2+} incorporation into the surface layer. The decrease of activation energy does not increase X_S (Fig. 1). Hence, the concentration factor–the density of "free" oxygen vacancies is more important than the energetic one.

For Pr-doped sample the effect of Pt supporting on E_a is the most complex, increasing it for some compositions and decreasing for others. At the highest doping level E_a is identical for samples with all dopants, agreeing with suggestion about changing the rate-limiting stage determined by the oxygen surface diffusion. A non-uniform distribution of Pt and Pr cations in/on the surface layer and domain boundaries might also affect paths of fast surface diffusion.

Activation energies of exchange were also estimated from the initial low-temperature parts of temperature-programmed exchange curves where the degree of exchange is small. In general, there is a reasonable correlation between the values of activation energy estimated by these two procedures as shown for Pr-doped samples in Fig. 3. The values of E_a estimated from the initial parts of exchange curves tend to be lower than those obtained by the Hall approach. This may be due to both a higher impact of steps occurring on Pt sites [16–18] as well as participation of defect sites with a lower oxygen bonding strength at lower temperatures.

Isothermal isotope exchange: For all samples, dependence of $\alpha(t)$ was close to the exponential one considered as indication on the identical reactivity of exchangeable oxygen forms [11–14]. This allowed to estimate specific rates of exchange R by using a simple integral form of Eq. (1). As follows from Fig. 4, dependence of these rates on the dopant content is similar to that of X_S. This agrees with conclusion that for Pt-supported samples dynamics of the oxygen heteroexchange is controlled by the surface diffusion step.

Activation energies estimated from the temperature dependence of specific rates of heteroexchange obtained in isothermal experiments in general correlate with values derived from results of TPIE experiments (Fig. 3).

To elucidate constants corresponding to the surface process and bulk diffusion, respectively, fitting of IIE data by solving the system of differential rate equations (1)–(4) following earlier verified approach [33] was made. Typical results of fitting are shown in Fig. 5. The rates of heteroexchange estimated from the integral equation and by fitting were found to be quite close. The share of the 3rd type of exchange varies from 0.85 to 0.93, i.e. close to

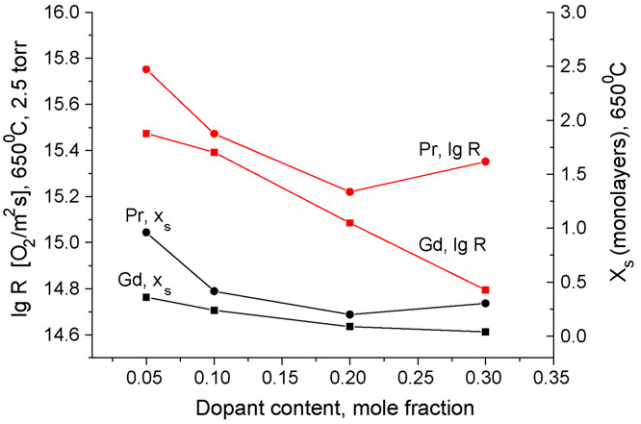

Fig. 4. The rate of oxygen heteroexchange and dynamic degree of exchange for Pr or Gd-doped Pt-supported Ce–Zr–O systems at 650 °C and 2.5 Torr O_2.

that estimated by isotope-mechanistic equation (vide supra). E_a of heteroexchange (~70 kJ/mole) was close to that estimated from IIE data by using an integral equation (~60 kJ/mole).

The values of oxygen self-diffusion coefficients D (10^{-15} to 10^{-16} m^2/s in studied temperature range) found by fitting are by 1–2 order of magnitude higher than the maximum values of D estimated for the near-surface layer for Pt/supported La–Ce–Zr–O sample (~10^{-17} m^2/s) from results of SSITKA experiments [33,36]. As expected, activation energy of bulk diffusion (~150 kJ/mol) is higher than that of the surface processes (vide supra).

4.2. Catalytic activity

Within each series with the same doping cation, catalytic activity in methane selective oxidation (Fig. 6) in diluted feeds correlates with concentration of Pt^{2+} species (and, hence, Pt dispersion) [5,7,20]. This is explained by a high efficiency of CH_4 molecules activation on dispersed oxidized Pt sites yielding H_2 and CO as primary products [5,31]. The difference in activity between the series of samples (Pr > Gd) in POM as well as in DR in diluted feed (Fig. 7) apparently correlates with the surface oxygen mobility characterized by X_S (vide supra). Hence, for the reactions characterized by moderate reducing/coking ability (POM, DR in diluted feed) dispersion of supported Pt seems to be more important factor than the oxygen mobility.

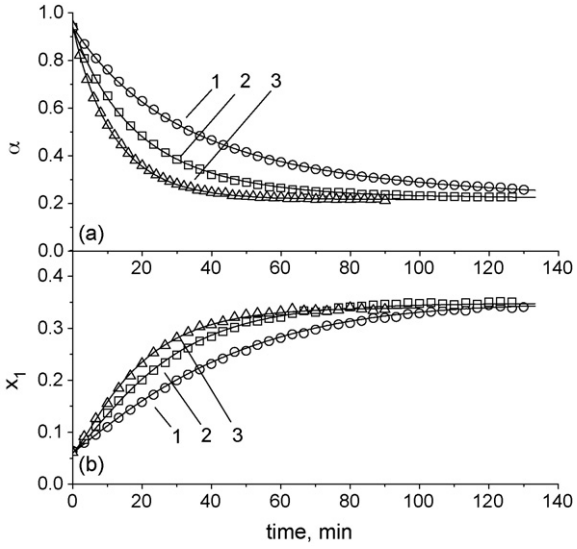

Fig. 5. Results of $\alpha(t)$ (a) $x_1(t)$ (b) fitting in isothermal isotope exchange at (1) 550 °C, (2) 600 °C and (3) 650 °C for Pt/$Pr_{0.3}Ce_{0.35}Zr_{0.35}$ sample.

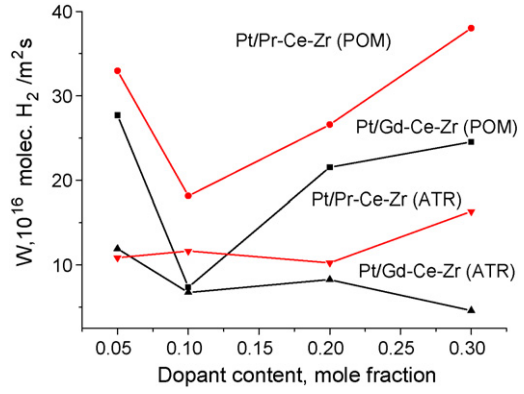

Fig. 6. Specific rates of H_2 formation for POM at 770 °C and acetone ATR at 880 °C.

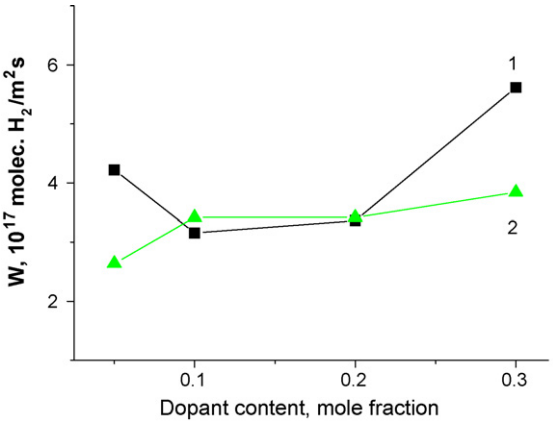

Fig. 7. Specific rates of H_2 formation for methane dry reforming at 770 C. 5 ms contact time, feed 1% CH_4 + 1% CO_2 in He. 1-Pt/$Pr_x(Ce_{0.5}Zr_{0.5})_{1-x}O_{2-y}$ samples and 2-Pt/$Gd_x(Ce_{0.5}Zr_{0.5})_{1-x}O_{2-y}$ samples.

In ATR of acetone characterized by more reducing reaction feed, catalytic performance correlates mainly with the oxygen mobility. This is explained by well-known excessive coking in this reaction counteracted by the oxygen mobility [26].

For the reaction of CH_4 dry reforming in concentrated feeds, correlation of activity with the surface oxygen mobility (X_S) and Pt dispersion (La > Pr > Gd [5]) is observed in the intermediate (up to

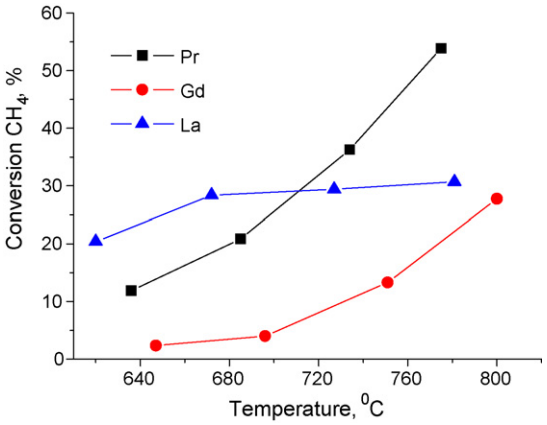

Fig. 8. Temperature dependence of CH_4 conversion in CH_4 DR for 1.4% Pt/$Ln_{0.3}$–Ce–Zr–O catalysts supported on walls of corundum channel. Feed composition 7% CH_4 + 7% CO_2 in He, contact time 15 ms.

650 °C) temperature range (Fig. 8). However, at higher (~800 °C) temperatures the order of activity is changed, and the highest performance is demonstrated by Pr-doped sample. This apparently correlates with the highest bulk oxygen mobility for this sample (vide supra). Since for dry reforming reaction in real feeds the main problem is coking leading to catalysts deactivation [24,25], this result implies that the bulk mobility in complex fluorite-like oxide supports is also an important factor favoring coke precursors gasification by supplying oxygen-containing species to the Pt-support interface.

5. Conclusions

For nanocrystalline Pt-supported ceria–zirconia samples doped with rare-earth (Gd, Pr, La) cations systematic comparison of parameters characterizing their oxygen mobility and reactivity estimated from the results of oxygen isotope exchange experiments in static installation in both isothermal (IE) and temperature-programmed modes (TPIE) using different analysis approaches has been made. Parameters characterizing exchange mechanism (type of exchange) and surface/near-surface oxygen mobility (dynamic degree of exchange X_S, E_a) can be estimated with a reasonable precision from results of high-throughput TPIE using simplified analysis procedures. However, estimation of the specific rates of exchange (especially with a due regard for steps occurring on supported Pt or Pt-support oxygen spillover stage) and bulk oxygen self-diffusion coefficient requires more detailed analysis of isothermal exchange experiments data solving the system of differential rate equations [33] or applying Monte Carlo simulation [36]. For partial oxidation and dry reforming of methane in diluted feeds, catalytic activity correlates both with Pt dispersion and oxygen mobility. Performance in acetone ATR and CH_4 DR in realistic feeds is mainly determined by the oxygen near surface and/or bulk mobility responsible for coking suppression.

Acknowledgements

This work was carried out in frames of Russian-French Associated European laboratory on catalysis. Support by OCMOL FP7 Project and RFBR–CNRS 09-03-93112 Project is gratefully acknowledged.

References

[1] J. Kašpar, P. Fornasiero, In catalysis by ceria and related materials, in: A. Trovarelli (Ed.), Catal. Sci. Ser., vol. 2, Imperial College Press, London, UK, 2002, pp. 217–241.
[2] H. He, H.X. Dai, L.H. Ng, K.W. Wong, C.T. Au, J. Catal. 206 (2002) 1.
[3] M. Mogensen, N.M. Sammes, G.A. Tompsett, Solid State Ionics 129 (2000) 63.
[4] V.A. Sadykov, Yu.V. Frolova, V.S. Muzykantov, V.P. Ivanov, H. Borhart, S. Neophytides, E. Kemnitz, K. Scheurell, Mater. Res. Soc. Symp. Proc. 835 (2005) 199.
[5] V. Sadykov, T.G. Kuznetsova, V.S. Muzykantov, L.G. Pinaeva, E.A. Paukshtis, N.V. Mezentseva, E. Kemnitz, C. Mirodatos, A.C. van Veen, Catal. Today 117 (2006) 475.
[6] V.A. Sadykov, N.V. Mezentseva, G.M. Alikina, A.I. Lukashevich, Yu.V. Borchert, T.G. Kuznetsova, V.P. Ivanov, E.A. Paukshtis, V.S. Muzykantov, V.L. Kuznetsov, V.A. Rogov, J. Ross, E. Kemnitz, C. Mirodatos, Solid State Phenomena 128 (2007) 239.
[7] V.A. Sadykov, T.G. Kuznetsova, G.M. Alikina, Yu.V. Frolova, A.I. Lukashevich, V.S. Muzykantov, V.A. Rogov, L.G. Ivanov, S. Pinaeva, E. Neophytides, K. Kemnitz, C. Scheurel, Mirodatos, in: D.K. McReynolds (Ed.), Book: New Topics in Catalysis Research, Nova Science Publishers, NY, USA, 2007, pp. 97–196 (Chapter 5).
[8] G.K. Boreskov, V.S. Muzykantov, Ann. N.Y. Acad. Sci. 213 (1975) 137.
[9] K. Klier, J. Novakova, P. Jiru, J. Catal. 2 (1963) 479.
[10] V.S. Muzykantov, G. Ewald, G. von Levis, Kinetika i Kataliz 15 (1974) 1512.
[11] V. Muzykantov, E. Kemnitz, V. Sadykov, V. Lunin, Kinetika i Kataliz 44 (2003) 349.
[12] V.S. Muzykantov, React. Kinet. Catal. Lett. 35 (1987) 437.
[13] V.S. Muzykantov, P. Jiru, K. Klier, Coll. Czech. Chem. Commun. 33 (1968) 829.
[14] G.K. Boreskov, Catalytic Activation of Dioxygen, Catalysis—Science and Technology, Springer, Berlin, 1982, v. 3 (Chapter 2).
[15] K. Klier, E. Kucera, J. Phys. Chem. Solids 27 (1966) 1087.
[16] A. Galdikas, C. Descorme, D. Duprez, Solid State Ionics 166 (2004) 147.
[17] A. Galdikas, D. Duprez, C. Descorme, Appl. Surf. Sci. 236 (2004) 342.
[18] D. Duprez, Isotopes in Heterogeneous Catalysis, Imperial College Press, London, 2006, p. 133.
[19] V. Sadykov, N. Mezentseva, G. Alikina, A. Lukashevich, V. Muzykantov, T. Kuznetsova, V. Ivanov, A. Boronin, A. Ishchenko, V. Rogov, J. Ross, E. Kemnitz, Mater. Res. Soc. Symp. Proc. 988 (2007), pp. QQ06–QQ04.
[20] V. Sadykov, V. Kriventsov, E. Moroz, Yu. Borchert, T. Kuznetsova, V. Ivanov, A. Boronin, N. Mezentseva, E. Burgina, J. Ross, Solid State Phenomena 128 (2007) 81.
[21] V. Sadykov, N. Mezentseva, V. Muzykantov, R. Bunina, A. Boronin, V. Voronin, I. Berger, Mater. Res. Soc. Symp. Proc. 1023 (2007) JJ02–07.
[22] T.G. Kuznetsova, V.A. Sadykov, Kinetics Catal. 49 (2008) 840.
[23] V. Sadykov, N. Mezentseva, V. Muzykantov, E. Gubanova, N. Sazonova, A. Bobin, V. Voronin, J. Ross, C. Mirodatos, Mater. Res. Soc. Symp. Proc. 1122 (2009), p. O05-O03.
[24] J.R.H. Ross, Catal. Today 100 (2005) 151.
[25] X.E. Verykios, Int. J. Hydrogen Energy 28 (2003) 1045.
[26] K. Takanabe, K. Aika, K. Seshan, L. Lefferts, Top. Catal. 49 (2008) 68.
[27] V. Sadykov, N. Mezentseva, G. Alikina, R. Bunina, V. Pelipenko, O. Bobrenok, A. Smirnova, J. Ross, O. Smorygo, B. Rietveld, Catal. Today 146 (2009) 132.
[28] F.J. Cheselske, W.E. Wallage, W.K. Hall, J. Phys. Chem. 63 (1959) 505.
[29] J. Wei, E. Iglesia, J. Phys. Chem. B 108 (2004) 4094.
[30] S. Pavlova, N. Sazonova, V. Sadykov, E. Gubanova, Catal. Today 105 (2005) 367.
[31] E.L. Gubanova, A. Van Veen, C. Mirodatos, V.A. Sadykov, N.N. Sazonova, Russ. J. Gen. Chem. 78 (2008) 2191.
[32] W.K. Hall, H.P. Leftin, F.J. Cheselske, D.E. O'Reilly, J. Catal. 2 (1963) 506.
[33] E. Sadovskaya, V. Sadykov, C. Mirodatos, J. Phys. Chem. A: Gen. 111 (2007) 4498.
[34] E. Mamontov, R. Brezny, M. Koranne, T. Egami, J. Phys. Chem. B 107 (2003) 13007.
[35] N. Bulgakov, V. Sadykov, V. Lunin, React. Kinet. Catal. Lett. 76 (2002) 103.
[36] D. Efremov, V. Sadykov, C. Mirodatos, Solid State Ionics 179 (2008) 847.